Boojums and the shapes of domains in monolayer films

Jiyu Fang, Ellis Teer, and Charles M. Knobler

Department of Chemistry and Biochemistry, University of California, Los Angeles, California 90095-1569

Kok-Kiong Loh and Joseph Rudnick

Department of Physics, University of California, Los Angeles, California 90095-1547

(Received 30 December 1996)

Domains in certain Langmuir monolayers support a texture that is the two-dimensional version of the feature known as a boojum. Such a texture has a quantifiable effect on the shape of the domain with which it is associated. The most noticeable consequence is a cusplike feature on the domain boundary. We report the results of an experimental and theoretical investigation of the shape of a domain in a Langmuir monolayer. A further aspect of the investigation is the study of the shape of a ''bubble'' of gaslike phase in such a monolayer. This structure supports a texture having the form of an *inverse* boojum. The distortion of a bubble resulting from this texture is also studied. The correspondence between theory and experiment, while not perfect, indicates that a qualitative understanding of the relationship between textures and domain shapes has been achieved. [S1063-651X(97)06407-6]

PACS number(s): 68.15.+e, 68.55.Ln, 68.18.+p, 68.60.−p

I. INTRODUCTION

The direct observation of monolayers at the air-water interface by the methods of polarized fluorescence microscopy (PFM) [1] and Brewster angle microscopy (BAM) [2] reveals that the films possess complex textures similar to those observed in liquid crystals. The textures are generally found in ''tilted'' phases, i.e., in phases in which the long axes of the molecules in the film are not perpendicular to the water surface but are uniformly tilted with respect to the normal. The textures are the result of the spontaneous organization of the molecular tilt azimuth on macroscopic length scales. They can be understood, at least qualitatively, in terms of continuum elastic theories of smectic liquid crystals [3].

Many striking textures have been found in domains of condensed tilted phases, such as the L_2 phase, that are surrounded by an isotropic phase, either liquid [often designated as liquid-expanded (L_1)] or gas (G) [4]. Among those textures are boojums, in which the tilt azimuth varies continuously and appears to radiate in some cases from a defect located at the edge of the domain and in others from a ''virtual'' defect in the isotropic phase [3,5]. The shapes of domains that contain the boojum texture are not round; they have a cusplike deformation pointing toward the defect.

In essence, the equilibrium shape of a domain containing a boojum is like the equilibrium shape of a crystal, which can be calculated with the use of the Wulff construction [6]. In that procedure it is assumed that the surface energy of the crystal is determined solely by the anisotropy of the bulk energy. For a monolayer domain containing a *nontrivial* texture this is not the case; the boundary (more properly, line) energy is comparable to the energy associated with the alignment of the tilt azimuth, so shape and texture must be calculated self-consistently.

Such a calculation has been performed by Rudnick and Bruinsma [7], who showed that there is a cusp on the domain boundary, quantified by an ''excluded'' angle Ψ that varies with R, the radius of the domain. Their results are displayed concisely in Fig. 1, which contains a pictorial definition of Ψ and a plot of Ψ versus $1/R$. The excluded angle is equal to zero when the domain is circular and increases as the cusp sharpens. Rudnick and Bruinsma predict that Ψ vanishes in the limit $R \rightarrow \infty$ and that the angle is initially linear in R^{-1}. The excluded angle goes through a maximum and then decreases to zero for sufficiently small domains. Schwartz
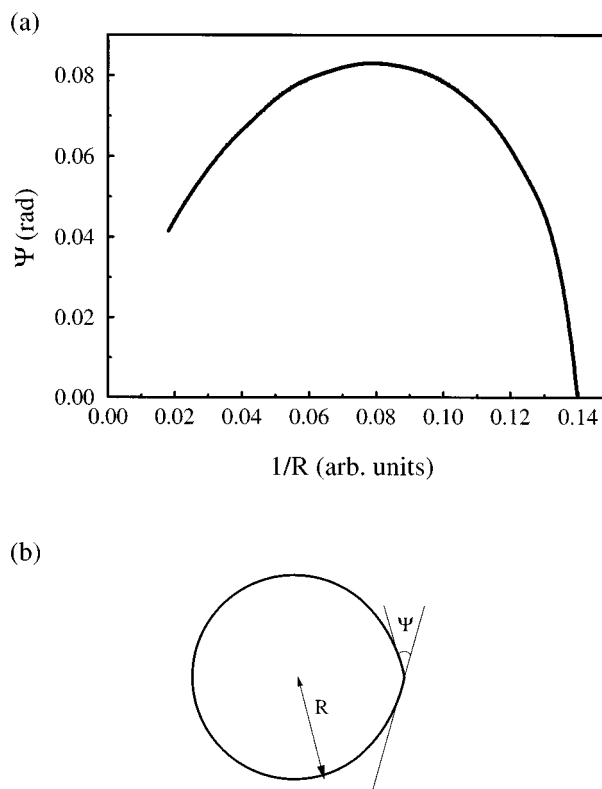

FIG. 1. (a) Excluded angle Ψ plotted as a function of $1/R$. (b) Definition of the excluded angle Ψ.

56   1859

et al. [8] made PFM measurements of Ψ for domains of pentadecanoic acid ranging in size from 12 to 120 μm. They found that the excluded angle increases with $1/R$, but roughly as a power law with an exponent of 0.3 rather than unity. There was no evidence of a maximum.

Rivière and Meunier [9] carried out BAM studies of condensed domains of hexadecanoic acid surrounded by a gaseous phase and measured the distance d of the virtual defect from the domain edge as a function of R. By assuming that the deformation of the domain is small, they were able to derive a relation between the quantity $\rho = d + R$ and the domain radius from continuum elastic theory. They compared the calculated and measured plots of ρ versus R and were able to obtain values for the ratio of the bend-splay elastic constant to the anisotropic part of the line tension. They also made a qualitative comparison between the measured elongation of the boojum-containing domains and the elongation calculated from a generalized Gibbs-Thompson equation that was obtained by Galatola and Fournier [10], this under the assumption that the texture is that of an undistorted boojum.

Experimental tests of the theory have been limited by the small range of domain sizes that could be examined by optical microscopy. In this paper we report measurements of the excluded angle for much smaller domains. This has been accomplished by transferring the monolayers to a solid support by the Langmuir-Blodgett technique and obtaining images with the use of scanning force microscopy. We also describe measurements on ''inverse'' boojums, which occur when there is a ''bubble'' of isotropic phase imbedded in a tilted phase. A theoretical analysis of the boojum problem, which is an extension and reformulation of the treatment of Rudnick and Bruinsma, is then described. Comparisons are made between the experiments and this theory.

II. EXPERIMENT

Monolayers of pentadecanoic acid (Nu-Chek Prep, $\geqslant$99%) were deposited from chloroform (Fisher spectranalyzed) solutions onto water (Millipore Milli-Q, pH 5.5) in a NIMA Type 611 trough. They were transferred onto mica substrates that had been freshly cleaved with adhesive tape and immediately inserted into the water subphase. The transfers were performed by withdrawing the mica from the subphase at constant speeds ranging from 0.5 to 2 mm/min. Boojums of the L_2 phase surrounded by the L_1 phase were obtained in the coexistence region at temperatures between 15 °C and 25 °C; boojums of the G phase surrounded by the L_2 phase were obtained in transfers at 7 °C.

The transferred monolayers were imaged with a scanning force microscope (SFM) (Park Scientific Instruments) using a 100-μm scanner at room temperature in ambient atmosphere. The instrument was calibrated on the micrometer scale by imaging grids with known spacings and on the nanometer scale with mica standards. A microfabrication triangular Si_3N_4 cantilever with a normal spring constant of 0.05 N/m was used for the measurements. The vertical bending and lateral torsion of the cantilever were monitored by reflecting a laser beam from the end of the cantilever onto a four-segment photodetector so that the topographic and frictional force images of the samples could be obtained simultaneously and independently of each other. All images were obtained in the constant-force mode. The loading forces ranged from 1 to 5 μN.

Brewster angle microscope images of Langmuir monolayers were obtained with an instrument of our own construction. Details of the instrument and the experimental procedures can be found elsewhere [11].

III. EXPERIMENTAL RESULTS

The key to the success of the experiment is the requirement that the boojums survive the transfer process and that their shape on the support be the same as that on the water surface. It has often been observed that the continuous L_1 phase breaks up into small islands when it is transferred to a solid support. The behavior has been found in monolayers of stearic acid deposited on thin polyethyleneimine films [12], dimyristolyphosphatidic acid deposited on glass [13], and octadecyltrichlorosilane deposited on acid-treated mica [14]. However, as can be seen in Fig. 2(a), despite the breakup of the L_1 phase, the boojum shapes of the L_2 phase survive. Langmuir-Blodgett transfer is also known to cause flow in monolayers [15,16], and there is evidence of this in the transfers made at 2 mm/min. As is evident in Fig. 2(b), the domains are elongated in the dipping direction. However, at 0.5 mm/min no distortion is evident and the boojums are not aligned in the dipping direcion.

A plot of the excluded angle against the reciprocal of the domain diameter is shown in Fig. 3. The same data are displayed in a log-log plot in Fig. 4. In the range 10–20 μm the data from the SFM studies agree with those obtained earlier by PFM [8]. We note that the slope of the log-log plot at large R is less than unity and that there is a nonzero intercept in the Ψ vs $1/R$ plot. The fact that the intercept is not zero had been overlooked in the earlier work, in which the data were presented on a log-log plot. By extending the measurements to smaller domains we have observed that there is a maximum and that the small domains become circular. There is no evidence of a cusp in domains smaller than 2 μm in diameter; see Fig. 2(c).

The good agreement between the PFM and SFM studies for the larger domains gives us confidence that the shapes have not been seriously changed during the transfer process or greatly affected by the change in substrate. We cannot be certain that this is true of the smaller domains, but it does seem likely that the effect of hydrodynamic flows and variations in the substrate will be most serious in the larger domains.

In the PFM studies [8] it was observed that inclusions of the L_1 phase in the L_2 domains also had cusps. When we examined films at temperatures below the L_1-L_2-G triple point at 13 °C [17], we found similar cusp-shaped regions in the isotropic G phase surrounded by the anisotropic L_2 phase. These domains also survive transfer to a solid support. Figure 5 is a frictional force image of such an inverse boojum. The frictional force within the inverse boojum is high because the tip images the mica substrate and not the dilute G phase. This is also confirmed by the topographic image, which was obtained simultaneously. The height profile shows that the inverse boojum extends to the substrate surface.
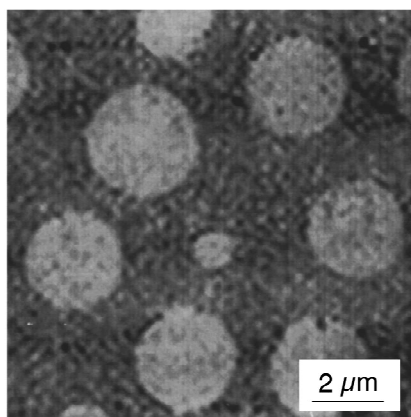
Measurements of the excluded angles in these inverse
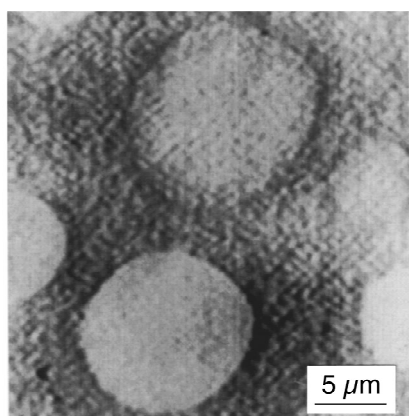
(a)
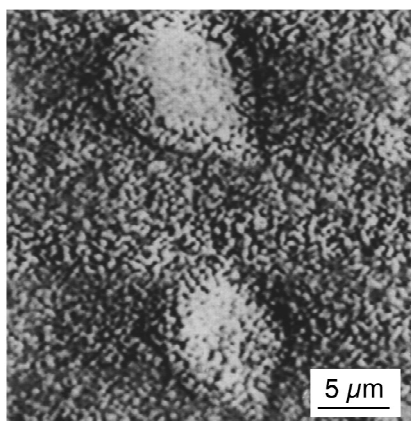
(b)

(c)

FIG. 2. Atomic force microscope images of domains associated with boojums. Monolayers were transferred onto mica from the L_2-L_1 coexistence region at a speed of (a) and (c) 0.5 mm/min, and (b) 2 mm/min.

boojums as a function of their radii are plotted in Fig. 6. The behavior is similar to that found for the ordinary boojums; the excluded angle has a nonzero intercept, increases roughly as $R^{-0.3}$, goes through a maximum and falls to zero. Included in the figure are three points obtained from BAM studies of inverse boojums in Langmuir monolayers of pentadecanoic acid. There is reasonable agreement with the SFM experiments for large domains. However, cusp angles are difficult to measure in small domains by BAM. They can
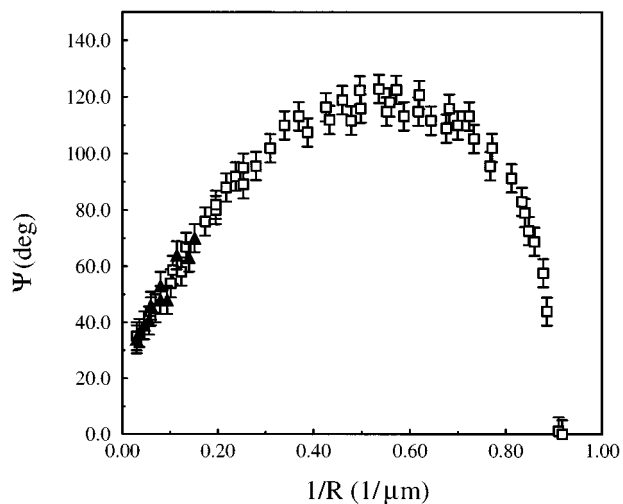

FIG. 3. Excluded angle of the cusplike feature on a domain supporting a boojum texture, plotted against the reciprocal of the domain radius. Filled triangles represent data for domains on the water surface and open squares represent data for domains tranferred onto mica.

be more easily and precisely measured by fluorescence microscopy, but the precipitation of the probe in the L_2-G two-phase region made this impossible.

IV. THE INVERSE BOOJUM

The boojum texture is an outcome of the competition between bulk and boundary energies in a bounded domain containing a condensed phase. When the boundary energy has the particular anisotropic form displayed below and the domain is a perfect circle, this texture is an exact solution to the energy minimization equations [7]. At the same time that the XY-like order parameter adjusts in response to the imperatives of energy minimization, the boundary also distorts so as to accommodate the now inhomogeneous environment presented by the texture. It has been found that when the energy
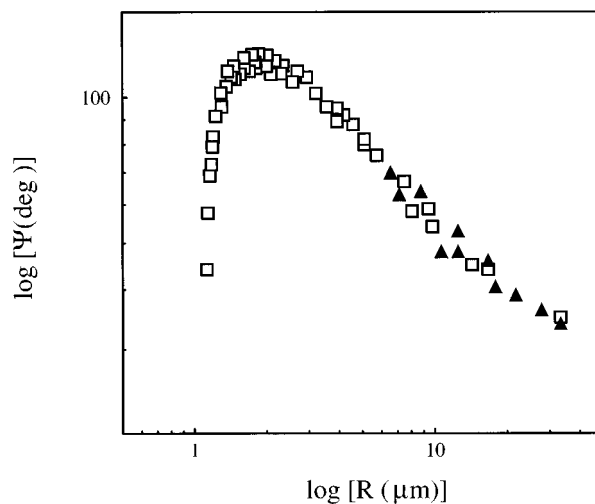

FIG. 4. A base-10 log-log plot of the dependence on radius of the excluded angle of the cusplike feature. Filled triangles represent data for domains on the water surface and open squares represent data for domains tranferred onto solid support.
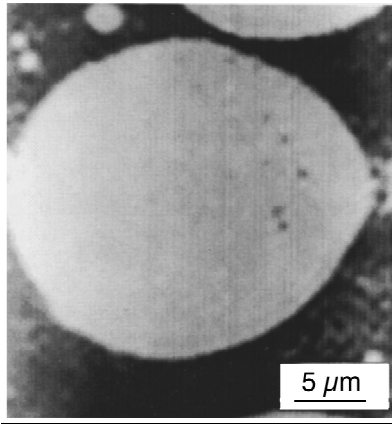
FIG. 5. Frictional force image of an inverse boojum consisting of a bubble of the isotropic G phase surrounded by the anisotropic L_2 phase. The monolayer was transferred onto mica from the L_2-G coexistence region at a speed of 0.5 mm/min.

is as given by Eqs. (4.1) and (4.4), a circular domain satisfies the extremum equations.

This means that the simple version of the energy of a domain in a Langmuir monolayer leads to a liquid-condensed-phase domain supporting a nontrivial texture whose boundary is perfectly circular. To explain the domain shapes observed in the experiments reported here and previously [8,9] it is necessary to introduce elaborations on the system's energy. The addition of a higher-order harmonic term to the line tension does give rise to a distortion of the boundary [7] and a feature in the form of a cusp appears. The theory is in qualitative accord with the experiments, except in the limiting large-domain behavior, where it predicts that the cusp angle vanishes rather than going to a limiting non-zero value as observed for both domains and bubbles.

The shapes of bubbles of an isotropic phase inside an ordered phase were not considered in the theory. When there
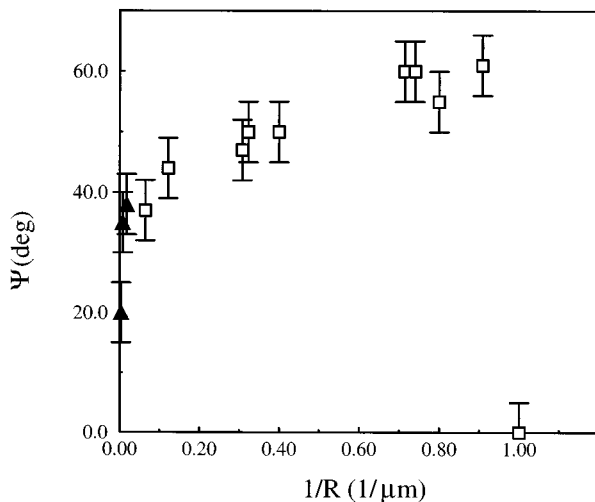

FIG. 6. Excluded angle of the cusps in bubbles of the isotropic G phase surrounded by the anisotropic L_2 phase, plotted against the reciprocal of the bubble radius. Filled triangles represent data for domains on the water surface and open squares represent data for domains transferred onto mica. Note the similarity to Fig. 3.

is a two-dimensional bubble of gas phase inside an extended region of the liquid-condensed phase, a texture appears in the liquid-condensed phase that is closely related to the virtual boojum observed in two-dimensional liquid-condensed droplets. This texture minimizes the total energy $H[\Theta(x,y)]$, given by

$$H[\Theta(x,y)] = \int_{\text{bulk}} \frac{\kappa}{2} |\vec{\nabla}\Theta|^2 dx \, dy$$

$$+ \int_{\text{boundary}} \sigma(\theta - \Theta(x,y)) ds, \quad (4.1)$$

where $\Theta(x,y)$ is the angle between the vector order parameter $\hat{c}$ and the x axis, while θ is the corresponding angle for the unit normal $\hat{n}$. The coefficient κ is the Frank or "spin stiffness" constant. The energy above follows from the assumption of equal bend and splay moduli, which is known to represent, at best, an approximation to physical reality. The function $\sigma(\theta - \Theta(x,y))$ is the surface energy, which depends on the relative orientations of $\hat{c}$ and the unit normal to the boundary $\hat{n}$. The extremum equations that arise are

$$\nabla^2 \Theta(x,y) = 0, \quad (4.2)$$

$$\kappa \frac{\partial \Theta}{\partial n} + \sigma'(\theta - \Theta) = 0. \quad (4.3)$$

Equation (4.2) applies outside the bubble and Eq. (4.3) at the interface. If $\sigma(\phi)$ has the form

$$\sigma(\phi) = \sigma_0 + a\cos\phi \quad (4.4)$$

and the bubble is a perfect circle, then a solution for $\Theta(x,y)$ that satisfies the extremum equations (4.2) and (4.3) is

$$\Theta(x,y) = \frac{1}{i}\left[\ln\left(1 - \frac{\alpha}{x - iy}\right) - \ln\left(1 - \frac{\alpha}{x + iy}\right)\right]. \quad (4.5)$$

Given the similarity between the mathematical structure of the right-hand side of Eq. (4.5) and the expression for $\Theta(x,y)$ in the case of the ordinary boojum (see Ref. [7]), this solution can be characterized as an INVERSE boojum. It is a texture with a singularity that lies a distance R_B from the origin, where

$$\frac{R_B}{R_0} = \frac{\alpha}{R_0} = \frac{aR_0/\kappa}{\sqrt{1 + (aR_0/\kappa)^2} + 1}. \quad (4.6)$$

The above relation serves to fix the value of the quantity α. Note that R_B is always less than the radius of the bubble. The singularity lies within the bubble. The texture associated with an inverse boojum is displayed in Fig. 7.
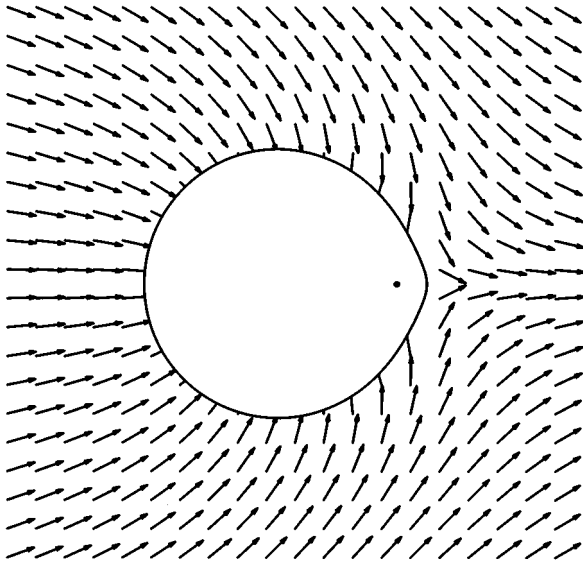
FIG. 7. Texture associated with an inverse boojum and the position of the virtual singularity, given by Eqs. (4.5) and (4.6). The distortion of the bubble from a circle, obtained from Eq. (5.24), is also indicated on the figure. The parameters used are $\kappa/a = 0.4 \ \mu$m, $a/\sigma_0 = 0.16$, and $R_0 = 2.4 \ \mu$m.

FIG. 8. Curves along which the order parameter points in a fixed direction in the immediate vicinity of a bubble. The parameters used are $\kappa/a = 0.4 \ \mu$m, $a/\sigma_0 = 0.16$, and $R_0 = 2.4 \ \mu$m.

When a boojum exists in a condensed-phase domain, the orientation of the director leads to an optical anisotropy that is observable by Brewster angle microscopy [8,9]. A ''sunburst'' of darker and lighter lines radiates from the point of singularity. Regions of constant intensity on the pattern correspond to portions of the texture in which the order parameter points in a fixed direction. In the case of the inverse boojum, there should be an analogous signature of the texture in the surrounding condensed phase. Using Eq. (4.5) one finds straightforwardly that the orientation of the order parameter is constant along the perimeter of a circle. This means that points of equal orientation fall on circular contours as shown in Fig. 8. The contours appear to pass through two points inside the bubble. One of the points is the location of the singularity and the other is the center of the bubble. The optical anisotropy that will be observed by BAM depends on the molecular parameters and the orientation of the boojum with respect to the direction of the incident light. Qualitative simulations of the images are shown in Fig. 9. They have been obtained by using the relation between tilt azimuth and reflectivity calculated by Tsao *et al.* [18]. These images can be compared with the BAM images in Fig. 10, which show similar variations in the reflectivity. It is interesting to note that the boojums appear to align. A similar alignment of isotropic droplets in a nematically ordered host phase has been observed [19]. This alignment is attributed to a long-range interaction produced by distortions in the director fields.

V. BUBBLE SHAPE: THEORY

In equilibrium a bubble takes on the shape that minimizes the system's free energy. If the interior is uniform and the line tension of an element of boundary depends on the orientation of the b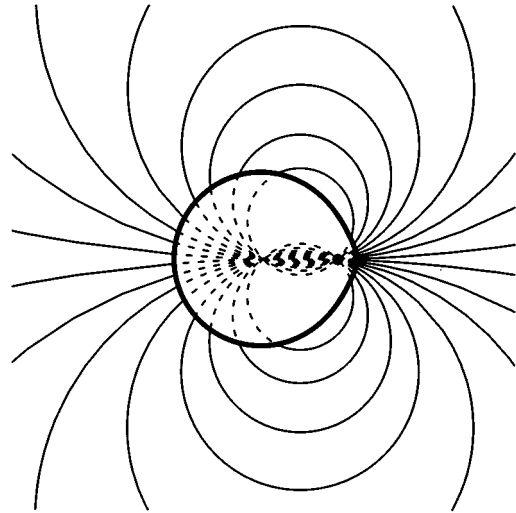oundary element, the Wulff construction can be utilized to yield the shape. In the case of inhomogenous interior structure, a generalized version of the Wulff construction provides an approach to the solution [7]. This method applies to the bubble in much the same way as it does to a domain. One discovers immediately that a circular bubble does *not* minimize the system energy of the form (4.1) with $\sigma(\phi)$ given by Eq. (4.4), in contrast to the result obtained for a domain [7] for which a circle represents the minimum-energy domain shape. However, the method cannot be applied directly because the curvature of the boundary changes sign. As a consequence, the radius of curvature of the boundary may become infinite at points along it, and this proves awkward in the context of the Wulff construction. However, a reparametrization allows one to proceed with the analysis. We find that there is no feature that can, strictly speaking, be described as a cusp, in that the slope of the bounding curve has no discontinuity. There is, on the other hand, a feature on the boundary whose shape can be quantified in terms of an excluded angle.

We have utilized an alternative approach to the determination of the bubble shape, to provide a check on our Wulff construction analysis. We adopt polar coordinates. This formulation confirms the results of the analysis based on the Wulff construction, and we are able to obtain explicit results for the bubble shape. Cusp angles may then be determined both analytically and by means of measurements on figures generated with the use of explicit analytical results, and these angles provide the basis for comparisons with experiment.

The remainder of this section consists of a review of the generalized Wulff construction, the development of the alternative approach, and a summary of results. Details are deferred to a future work [20].

A. Generalized Wulff construction

Following the approach of Rudnick and Bruinsma, we attempt to apply the generalized Wulff construction [7] to determine the shape of the bubble. In our application, this
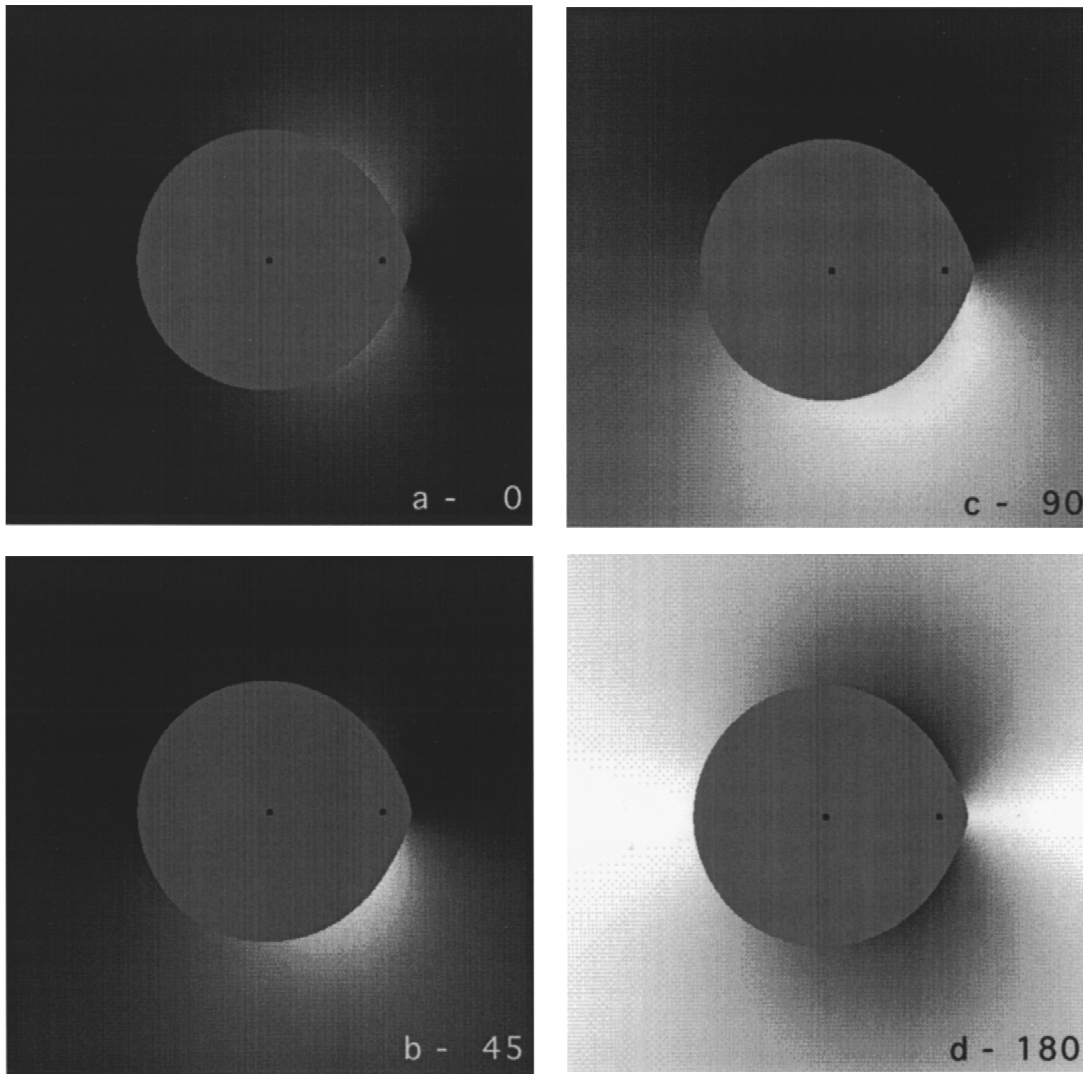
FIG. 9. Simulated BAM images of inverse boojums for different orientations with respect to the incident light. The orientation of the beam with respect to the symmetry axis of the boojum is specified in the lower corner of each figure.

technique is used to minimize the total energy Eq. (4.1) with respect to the Burton-Cabrera-Frank (BCF) parametrization of bubble shape, i.e., $R(\theta)$ and θ [21].

We rederive the Wulff construction so as to remove the approximation, utilized in earlier work [7], that the radius of curvature $R + R''$ is constant. We obtain

$$\frac{\delta}{\delta R}\int_{\text{bulk}}\frac{\kappa}{2}|\vec{\nabla}\Theta|^2 dx\ dy = -\frac{\kappa}{2}|\vec{\nabla}\Theta|^2[R+R''].\quad (5.1)$$

It can be shown that if $\sigma(\phi)=\sigma(-\phi)$, we have for the bubble

$$\frac{\delta}{\delta R}\int_{\text{boundary}}\sigma(\theta-\Theta(x,y))ds = \sigma+\sigma''-(R+R'')\left[\sigma'\left(\cos\theta\frac{\partial}{\partial x}+\sin\theta\frac{\partial}{\partial y}\right)+\sigma''\left(-\sin\theta\frac{\partial}{\partial x}+\cos\theta\frac{\partial}{\partial y}\right)\right]\Theta.\quad (5.2)$$

If we adopt Eqs. (4.4) and (4.5), the equation for the shape of the bubble is given by

$$\frac{\delta H}{\delta R}=0\Rightarrow r+r''=\frac{(1-2\alpha\cos\theta+\alpha^2)^2}{2\alpha(\alpha+\delta)\cos 2\theta-4\alpha(1+\alpha^2+2\delta\alpha)\cos\theta+1+4\alpha^2+\alpha^4+\delta\alpha(1+6\alpha^2-\alpha^4)},\quad (5.3)$$
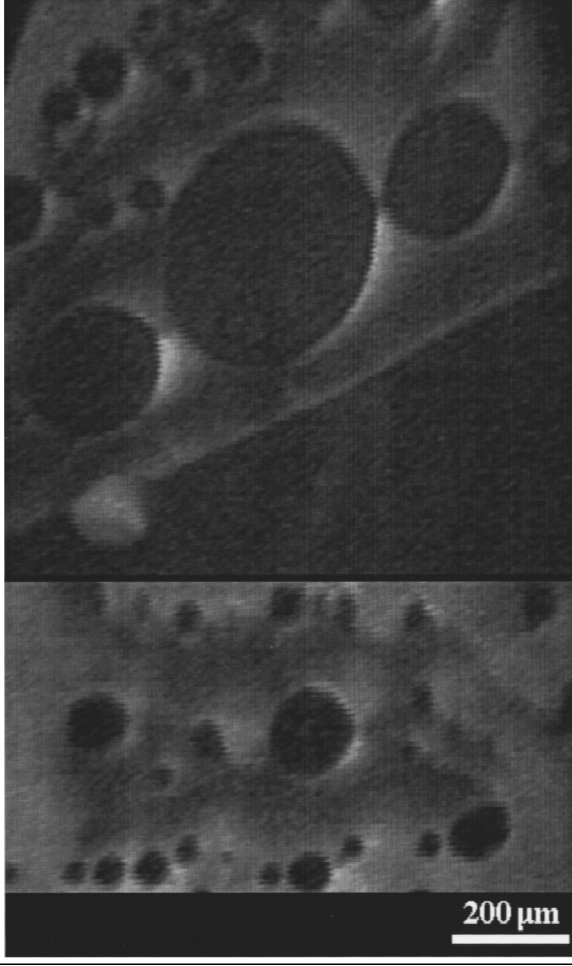
FIG. 10. BAM images of inverse boojums in Langmuir mono-layers of pentadecanoic acid at 5 °C.

where $\delta = a/\sigma_0$, $R = R_0 r$, and R_0 is the radius of the unperturbed circle. The denominator of Eq. (5.3) passes through zero in regimes of interest, and this complicates the analysis. It proves useful to reparametrize the system in Cartesian coordinates.

The relations between the parametrization using Cartesian coordinates and the BCF parametrization are

$$x = r\sin\theta + r'\cos\theta, \qquad (5.4)$$

$$y = r\cos\theta - r'\sin\theta. \qquad (5.5)$$

Using Eqs. (5.4) and (5.5), we have the following relations for nearly circular boundaries in the region where θ is small:

$$\frac{1}{r + r''} = -\frac{y''}{\sqrt{1 + y'^2}^3} \approx -y'', \qquad (5.6)$$

$$\cos\theta \approx \sqrt{1 - x^2} \approx 1 - \frac{x^2}{2} - \frac{x^4}{8}. \qquad (5.7)$$

Substituting Eqs. (5.6) and (5.7) into Eq. (5.3), we obtain

$$y'' = -\frac{C_2(x^2 - k_+)(x^2 - k_-)}{[\alpha x^2 + (1-\alpha)^2]^2}, \qquad (5.8)$$

where

$$k_\pm = \frac{-C_1 \pm \sqrt{C_1^2 - 4C_0 C_2}}{2C_2}, \qquad (5.9)$$

$$C_2 = \frac{\alpha}{2}(1 + \alpha^2 + 2\delta\alpha), \qquad (5.10)$$

$$C_1 = 2\alpha(1-\alpha)^2 - 4\delta\alpha(1-\alpha), \qquad (5.11)$$

$$C_0 = (1-\alpha)^4 + \delta\alpha(3+\alpha)(1-\alpha)^3. \qquad (5.12)$$

The integration of Eq. (5.8) is readily performed and yields

$$
\begin{aligned}
y' = &-\frac{C_2 x}{\alpha^2} \\
&- \frac{C_2(1-\alpha)^4 - C_1\alpha(1-\alpha)^2 + C_0\alpha^2}{2\alpha^2(1-\alpha)^2} \frac{x}{(1-\alpha)^2 + \alpha x^2} \\
&+ \frac{3C_2(1-\alpha)^4 - C_1(1-\alpha)^2 - C_0\alpha^2}{2(1-\alpha)^3\alpha^{5/2}}\tan^{-1}\frac{\alpha^{1/2}x}{1-\alpha} + K_{y'},
\end{aligned}
$$

$$(5.13)$$

and

$$
\begin{aligned}
y = &-\frac{C_2 x^2}{2\alpha^2} - \frac{2(1-\alpha)^2 + C_1\alpha}{2\alpha^3}\ln[\alpha x^2 + (1-\alpha)^2] \\
&+ \frac{3C_2(1-\alpha)^4 - C_1(1-\alpha)^2 - C_0\alpha^2}{2(1-\alpha)^3\alpha^{5/2}}x\,\tan^{-1}\frac{\alpha^{1/2}x}{1-\alpha} \\
&+ K_{y'}x + K_y.
\end{aligned}
$$

$$(5.14)$$

The next step is to fix the constants of integration $K_{y'}$ and K_y. Symmetry requires $y'(-x) = -y'(x)$ and yields $K_{y'} = 0$. The bounding curve $y(x)$ will merge into a circle of radius 1, centered at the origin. The merging point $(x_0, y(x_0))$ is taken to be the point at which $y'(x_0) = -x_0/\sqrt{1-x_0^2}$. This leads to

$$
\begin{aligned}
K_y = &\frac{C_2 x_0^2}{2\alpha^2} + \frac{2(1-\alpha)^2 + C_1\alpha}{2\alpha^3}\ln[\alpha x_0^2 + (1-\alpha)^2] \\
&- \frac{3C_2(1-\alpha)^4 - C_1(1-\alpha)^2 - C_0\alpha^2}{2(1-\alpha)^3\alpha^{5/2}}x_0\tan^{-1}\frac{\alpha^{1/2}x_0}{1-\alpha} \\
&+ \sqrt{1 - x_0^2}.
\end{aligned}
$$

$$(5.15)$$

The boundary of the bubble (5.14) is smooth in that there is no discontinuity in the slope of the bounding curve. For very small R_0, the radius of curvature of the boundary close to the singularity $b = 1/y''(0)$ is approximately equal to R_0. The bubble appears to be circular and the excluded angle Ψ is zero. The ratio $\beta = b/R_0$ decreases as R_0 increases. This causes the bubble to sharpen at one end. When β exceeds a critical value β_c, this sharper end has properties in common with a cusp and one is able to derive an excluded angle Ψ, as depicted in Fig. 11(a). It can be shown that Ψ is given by the
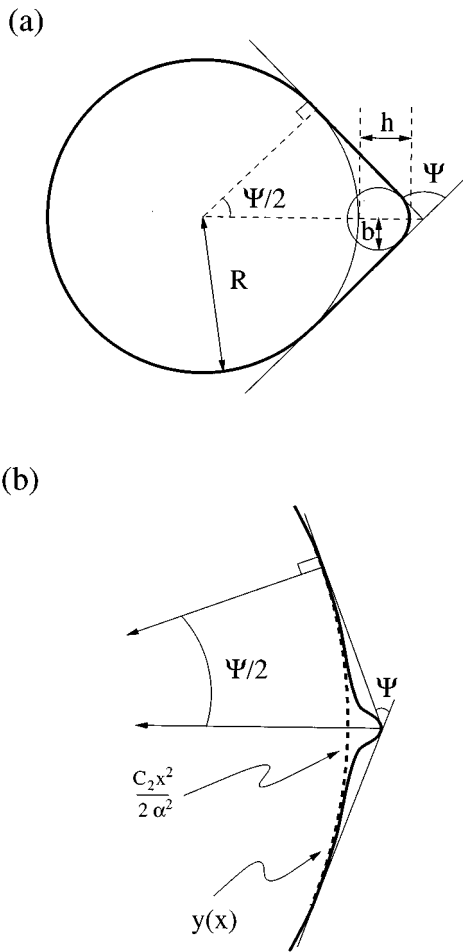
(a)

(b)

FIG. 11. (a) The way in which Ψ is defined where the boundary is smooth. This method leads to an analytical expression for the excluded angle of a cusplike feature. (b) For $R_0 \gg \kappa/a$, the cusplike feature shows up differently and requires a new definition of Ψ.

$$\Psi = 2 \cos^{-1} \frac{1}{1 + \dfrac{h}{1 - b}}, \qquad (5.16)$$

where $h = |y(0) + 1|$ is the deviation of the tip of the feature from a circle. Because there is never a cusp in the strict sense of the term, the choice of β_c is a matter of individual judgement. Based on theoretical bubble shapes obtained in Fig. 12, β_c is chosen to be 0.45.

When $R_0 \gg \kappa/a$, the x^2 term in Eq. (5.14) dominates. The boundary around the cusplike feature is this x^2 term instead of the unperturbed circle. The new definition of the excluded angle is as displayed in Fig. 11(b), and we find that Ψ can be expressed as

$$\Psi \approx 2 \sqrt{2 \left| \frac{2(1-\alpha)^2 + C_1 \alpha}{\alpha^3} \ln(1-\alpha) \right|}. \qquad (5.17)$$

In this limit $\alpha \to 1 - \epsilon$, where $\epsilon \propto r^{-1} \ll 1$, we approximate C_1 as

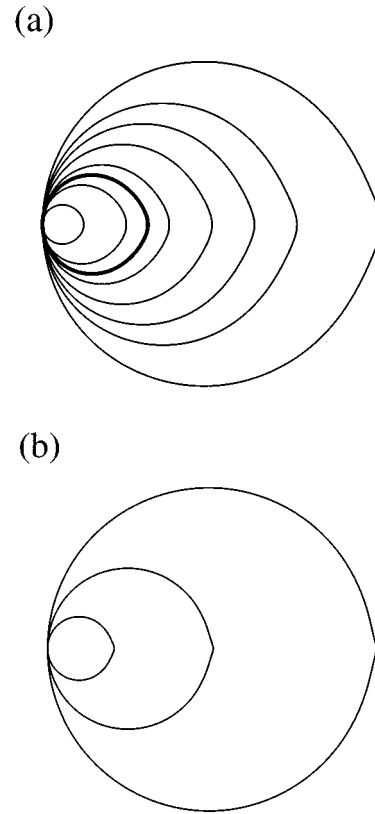$$C_1 \approx 2\epsilon(\epsilon - 2\delta) + O(\delta\epsilon^2). \qquad (5.18)$$

(a)

(b)

FIG. 12. (a) Calculated shapes for bubbles with $R_0 = 0.4$, 0.8, 1, 1.2, 1.6, 2, 2.4, and 3.2 μm. The bubble that is drawn as the thicker line is the one of the nominal size $R_c = 1$ μm when $\beta_c = 0.45$. (b) Calculated shapes for the bubbles of $R_0 = 3.2$, 8, and 16 μm . The parameters used are $\kappa/a = 0.4$ μm and $a/\sigma_0 = 0.16$.

We then have the large-R_0 behavior of the excluded angle

$$\Psi \approx 2 \sqrt{\frac{8\kappa}{\sigma_0 R_0} \left| \ln \frac{\kappa}{aR_0} \right|}. \qquad (5.19)$$

B. Polar coordinates

As an alternative, one can parametrize the domain boundary in polar coordinates. In this case, we choose an origin, nominally at the center of the undistorted circular bubble. The Cartesian coordinates x and y are replaced by r, the distance from the origin, and ϕ, the angle with respect to the x axis. In terms of r and ϕ, the inverse boojum texture has the form

$$\Theta(r,\phi) = \frac{1}{i} \left[\ln\left(1 - \frac{\alpha}{r}e^{i\phi}\right) - \ln\left(1 - \frac{\alpha}{r}e^{-i\phi}\right) \right]. \qquad (5.20)$$

The boundary condition (4.3) leads to a previously quoted result for the parameter α,

$$\frac{\alpha}{R_0} = \frac{1}{\sqrt{(\kappa/\alpha R_0)^2 + 1} + (\kappa/\alpha R_0)}, \qquad (5.21)$$

where R_0 is the radius of the circular bubble. In fact, Eq. (5.20) is just Eq. (4.5) expressed in polar coordinates and Eq.

(5.21) is identical to Eq. (4.6). The parameter α has a simple interpretation: it is the distance of the singularity associated with the virtual boojum from the center of the bubble. Note that, according to Eq. (4.6), the singularity always lies within the bubble.

We now proceed with a calculation of the distortion of the bubble from a circle. Our results are the leading-order terms in an expansion in the dimensionless, and presumably small, combination a/σ_0. If one writes

$$r(\phi) = R_0 e^{k(\phi)}, \tag{5.22}$$

one eventually arrives at

$$R_0 \sigma_0 k''(\phi) = -a\alpha \left[\left(e^{i\phi} - \frac{\alpha}{R_0} \right) e^{i\phi} \bigg/ \left(1 - \frac{\alpha}{R_0} e^{i\phi} \right)^2 \right.$$
$$\left. + \left(e^{-i\phi} - \frac{\alpha}{R_0} \right) e^{-i\phi} \bigg/ \left(1 - \frac{\alpha}{R_0} e^{-i\phi} \right)^2 \right]$$
$$- \frac{2\kappa \left(\dfrac{\alpha}{R_0} \right)^2}{\left(1 - \dfrac{\alpha}{\rho} e^{i\phi} \right) \left(1 - \dfrac{\alpha}{\rho} e^{-i\phi} \right)}. \tag{5.23}$$

Equation (5.23) represents the leading term in an expansion in the dimensionless combination a/σ_0. This ratio is small, as the line tension is assumed to be nearly isotropic.

The double integration of Eq. (5.23) is relatively straightforward. One finds for $k(\phi)$

$$k(\phi) = \frac{2\kappa}{\sigma_0 R_0}$$
$$\times \left\{ 2 \int_{-\pi}^{\phi} \arctan \left[\frac{\alpha}{R_0} \sin\phi' \bigg/ \left(1 - \frac{\alpha}{R_0} \cos\phi' \right) \right] d\phi' \right.$$
$$\left. - \ln \left[1 + \left(\frac{\alpha}{R_0} \right)^2 - 2\frac{\alpha}{R_0} \cos\phi \right] + 2\ln \left(1 + \frac{\alpha}{R_0} \right) \right\}. \tag{5.24}$$

In the regimes in which comparisons can be made, the results of the calculation based on the utilization of polar coordinates are in complete accord with those that follow from the Wulff construction. In addition, an analysis based on polar coordinates, in particular Eq. (5.24), can provide figures that can be utilized for comparison with experimental data. Bubbles whose shapes are described by Eqs. (5.22) and (5.24) are displayed in Fig. 12. These bubbles comprise the results of theoretical modeling that are compared with the data described in earlier sections.

VI. RESULTS AND CONCLUSIONS

We now compare the theoretical excluded angles with the experimental ones. Equation (5.16) provides the basis for comparison between experiments and theory. We find that the best fit is achieved when the parameters are chosen as $\kappa/a = 0.4$ μm and $a/\sigma_0 = 0.16$. The comparison between theory and experiment is displayed in Fig. 13. Because there is never a cusp in the form of a discontinuity in the slope of
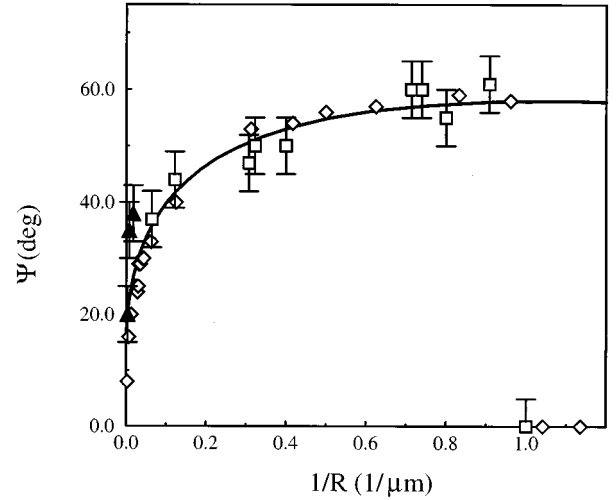

FIG. 13. Comparison between experimental and calculated excluded angles. The experimentally measured excluded angle of the cusps in bubbles are shown as filled triangles and open squares as in Fig. 6 and excluded angles measured on the calculated bubbles are shown as open diamonds. The solid line represents the analytic expression of the theoretical excluded angle. Note the fundamental difference between the behavior of the theoretical curve for $R \to 0$, which tends monotonically to a finite limit, and the measured excluded angle of calculated bubbles, which seems to rise rapidly from zero as the bubble radius exceeds a "threshold" value.

the bounding curve, we are unable to definitively model the "onset" of a cusp. However, we do find an apparent rapid dropoff to zero of the (nominal) excluded angle. Furthermore, the theory predicts that sufficiently small bubbles will be *nearly* circular. With the exercise of a little judgement, it is possible to determine a value of what appears to be the radius of onset R_c. For the parameters of choice, we find $R_c = 1 \mu$m for $\beta_c = 0.45$.

Our theory appears to reproduce fairly well both the qualitative and the quantitative behavior of the bubble shapes as a function of the bubble size. Small bubbles are nearly circular and the excluded angle Ψ is equal to zero. Cusplike features are observed for bubbles having radii R_0 greater than a threshold value R_c. The angle Ψ decreases for bubbles of larger sizes. However, in the experiments the excluded angle Ψ tends to a nonzero constant as $R_0 \to \infty$. This limiting behavior is not achievable within the framework of the theory presented here. It is known that thermal fluctuations will cause the line tension coefficients to depend on the diameter of the bubble or domain [22]. However, preliminary calculations indicate that this renormalization has no effect on the asymptotic behavior of the excluded angle for large bubbles. A possible source of the discrepancy is the difference between the bend and splay moduli, which has been neglected in the present work.

The ratio κ/a for hexadecanoic acid has been obtained by Rivière and Meunier [9]. They find 28 μm$< \kappa/a <$40 μm, which is about two orders of magnitude larger than our best estimate $\kappa/a = 0.4$ μm . Studies of other textures in monolayers such as stripes [23] indicate that κ increases with chain length. This could account for some of the difference. Another possible reason for this discrepancy is the fact that Rivière and Meunier adopted $\kappa_1 \neq \kappa_3$ as the basis for texture

distortions while we have used a, the anisotropic line tension, as the mechanism for bubble shape distortions. Our comparison between theory and experiment gives an estimate of $a/\sigma_0 = 0.16$ for pentadecanoic acid at the liquid-condensed–gas boundary. The line tension anisotropy, which corresponds to our a/σ_0, has been estimated for the liquid-condensed–liquid-expanded interface in D-myristoyl alanine from studies of dendritic growth [24]. The value found is 0.005–0.025. Given the fact that the systems are not identical and that these are only estimates of the anisotropy, the difference is not disturbing.

In summary, we have formulated a theory for bubbles in Langmuir monolayers that is an extension and reformulation of the theory of domain shapes discussed by Rudnick and Bruinsma [7]. Although the current theory predicts a smooth bubble boundary, there exist cusplike features with well-defined and measurable excluded angles when the radius of the bubble exceeds a nominal value R_c. Comparing theoretical excluded angles with the results of experiments, we find good qualitative and quantitative agreement. However, there are also discrepancies. Experimental observations and related work indicate that the difference between κ_1 and κ_3 cannot be neglected. The calculation of an equilibrium texture when $\kappa_1 \neq \kappa_3$ is currently being performed as a prelude to the determination of the shape of a bubble or domain.

[1] V. T. Moy, D. J. Keller, H. E. Gaub, and H. M. McConnell, J. Phys. Chem. **90**, 3198 (1986); D. K. Schwartz and C. M. Knobler, *ibid.* **97**, 8849 (1993).

[2] S. Hénon and J. Meunier, Rev. Sci. Instrum. **62**, 936 (1991); D. Hönig and D. Möbius, J. Phys. Chem. **95**, 4590 (1991).

[3] T. Fischer, C. M. Knobler, and R. Bruinsma, Phys. Rev. E **50**, 423 (1994).

[4] For a description of monolayer phases see C. M. Knobler and R. C. Desai, Annu. Rev. Phys. Chem. **43**, 207 (1992).

[5] S. A. Langer and J. P. Sethna, Phys. Rev. A **34**, 5035 (1986). For the original discussion of boojums see N. D. Mermin, in *Quantum Fluids and Solids*, edited by S. B. Trickey, E. Adams, and J. Duffy (Plenum, New York, 1977).

[6] G. Wulff, Z. Kristallogr. **34**, 449 (1901); M. Wortis, in *Chemistry and Physics of Solid Surfaces VII*, edited by R. Vanselow and R. Howe (Springer-Verlag Berlin, 1988), p. 367.

[7] J. Rudnick and R. Bruinsma, Phys. Rev. Lett. **74**, 2491 (1995).

[8] D. K. Schwartz, M.-W. Tsao, and C. M. Knobler, J. Chem. Phys. **101**, 8258 (1994).

[9] R. Rivière and J. Meunier, Phys. Rev. Lett. **74**, 2495 (1995).

[10] P. Galatola and J. B. Fournier, Phys. Rev. Lett. **75**, 3297 (1995).

[11] B. Fischer, M.-W. Tsao, J. Ruiz-Garcia, T. M. Fischer, and C. M. Knobler, J. Phys. Chem. **98**, 7430 (1994).

[12] L. F. Chi, M. Anders, H. Fuchs, R. R. Johnston, and H. Ringsdorf, Science **259**, 213 (1993).

[13] J. M. Mikrut, P. Dutta, J. B. Ketterson, and R. C. MacDonald, Phys. Rev. B **48**, 14 479 (1993).

[14] J. Y. Fang and C. M. Knobler, J. Phys. Chem. **99**, 10 425 (1995).

[15] S. Schwiegk, T. Vahlenkamp, Y.-Z. Xu, and G. Wegner, Macromolecules **25**, 2513 (1992).

[16] J. Y. Fang, Z. H. Lu, G. W. Min, Z. M. Ai, Y. Wei, and P. Stroeve, Phys. Rev. A **46**, 4963 (1992).

[17] B. G. Moore, C. M. Knobler, S. Akamatsu, and F. Rondelez, J. Phys. Chem. **94**, 4588 (1990).

[18] M.-W. Tsao, T. M. Fischer, and C. M. Knobler, Langmuir **11**, 3184 (1995).

[19] P. Poulin, H. Stark, T. C. Lubensky, and D. A. Weitz, Science **275**, 1770 (1997).

[20] K. K. Loh and J. Rudnick (unpublished).

[21] W. K. Burton, N. Cabrera, and F. C. Frank, Philos. Trans. R. Soc. London, Ser. A **243**, 291 (1951).

[22] H. Saleur and P. Fendley (private communication).

[23] J. Ruiz-Garcia, X. Qiu, M.-W. Tsao, G. Marshall, and C. M. Knobler, J. Phys. Chem. **97**, 6955 (1993).

[24] S. Akamatsu, O. Bouloussa, K. To, and F. Rondelez, Phys. Rev. A **46**, 4504 (1992).